International Journal of Nanomedicine

Dovepress
open access to scientific and medical research

Open Access Full Text Article

ORIGINAL RESEARCH

Protective Effects of Carbon Dots Derived from *Armeniacae Semen Amarum* Carbonisata Against Acute Lung Injury Induced by Lipopolysaccharides in Rats

Yusheng Zhao[1]
Yue Zhang[2]
Hui Kong[1]
Guoliang Cheng[1]
Huihua Qu[3]
Yan Zhao[1]

[1]School of Traditional Chinese Medicine, Beijing University of Chinese Medicine, Beijing, 100029, People's Republic of China; [2]School of Life Sciences, Beijing University of Chinese Medicine, Beijing, 100029, People's Republic of China; [3]Centre of Scientific Experiment, Beijing University of Chinese Medicine, Beijing, 100029, People's Republic of China

Introduction: The charcoal processed product of *Armeniacae Semen Amarum* (ASA), ASA Carbonisata (ASAC), has long been used for its anti-inflammatory effects. However, the material basis and mechanism of action of ASAC remain unclear.

Aim: To explore the anti-inflammatory effects of *Armeniacae Semen Amarum* Carbonisata-derived carbon dots (ASAC-CDs).

Methods: The physicochemical properties of ASAC-CDs including morphology, optical properties, functional groups were characterized by a series of methods, mainly including electron microscopy, optical technology and X-ray photoelectron spectroscopy. The anti-inflammatory effect of ASAC-CDs was evaluated and confirmed using acute lung injury (ALI) induced by lipopolysaccharides (LPS) in rats.

Results: The ASAC-CDs ranged from 1.5 to 5.5 nm in diameter, with a quantum yield of 3.17%. ASAC-CDs alleviated LPS-induced inflammation, as demonstrated by reducing the levels of IL-6, IL-1β and TNF-α and increasing the contents of IL-10 in rat serum. More interestingly, ASAC-CDs reduce the content of MDA and MPO and increase the activity of SOD and the content of GSH, indicating the antioxidant activity of ASAC-CDs.

Conclusion: These results demonstrate the remarkable anti-inflammatory effects of ASAC-CDs against ALI induced by LPS, which provide an important basis for the application of ASAC-CDs in clinical anti-pneumonia, and lay an experimental foundation for the research and development of novel nano-drugs.

Keywords: *Armeniacae Semen Amarum* Carbonisata, carbon dots, lipopolysaccharide, anti-inflammatory

Introduction

Acute lung injury (ALI) is a life-threatening medical disease with high morbidity and mortality. ALI refers to the damage of alveolar epithelial cells and pneumonic capillary endothelial cells caused by non-cardiogenic variables.[1] The clinical appearances are respiratory trouble and headstrong hypoxemia, which can further develop into intense respiratory trouble disorder.[2] ALI can lead to intemperate irritation, a huge number of neutrophils penetrate the lung tissue, and advance the discharge of inflammation cytokines and damage of lung endothelial cells and epithelial cells.[3] Lipopolysaccharide (LPS), moreover known as endotoxin, is the most component of the external film of gram-negative microscopic organisms.[4] It has critical pathogenicity and is one of the imperative

Correspondence: Huihua Qu; Yan Zhao
Tel +86 10 6428 6705
Fax +86 1 6428 6821
Email quhuihuadr@163.com; zhaoyandr@163.com

Received: 14 October 2021
Accepted: 14 December 2021
Published: 4 January 2022

Graphical Abstract

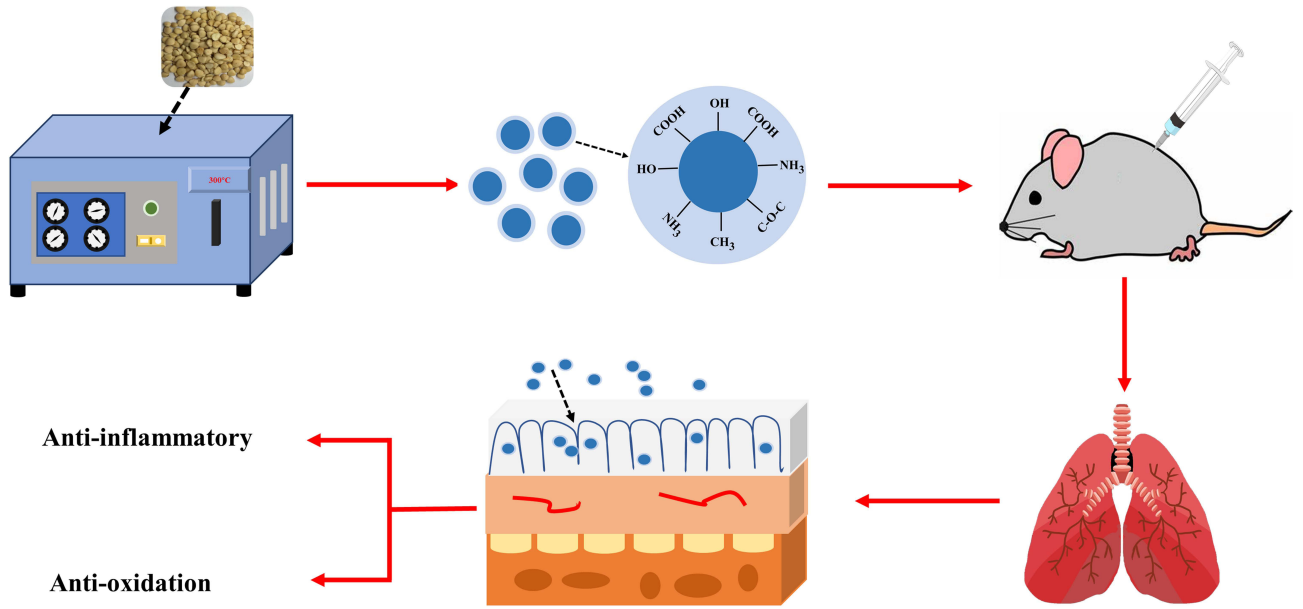

causes of ALI.[5] The existing drugs for the treatment of ALI are corticosteroid drugs, but these drugs frequently cause serious side impacts. Hence, the improvement of a possibly secure and compelling drug without side impacts is of awesome noteworthiness for the treatment of ALI.

As one of the developing nanomaterials, carbon dots (CDs) have surprising execution compared to other nanomaterials, such as ultra-fine size, predominant photoluminescence, multifunctional surface, and adjustable chemical properties.[6–8] Additionally, excessive evidences detailed CDs derived distinctive precursors[9,10] or preparing conditions[11,12] appeared diverse properties, primarily performed on the aspects of size, charge and chemical groups. These contrasts in properties have been illustrated to be closely associated with the bioactivities of CDs, which advance given a sound clarification for the reality that CDs right now found had diverse activities including anti-hemorrhagic,[13] anti-inflammation[14] and antioxidant.[15] Based on this, the unfamiliar and study-worthy possibilities of CDs for controlling or treating other illnesses such as ALI gets to be the centre of current investigation, which merited to be conducted.

Armeniacae Semen Amarum (ASA) is the dried mature seeds of *Prunus armeniaca L.var. ansu Maxim, Prunus sibirica L, Prunusm andshurica (Maxim.) Koehne or Prunus armeniaca L*. As a traditional Chinese medication (TCM) broadly utilized in China, ASA was to begin with recorded as a drug in *Sheng Nong's Herbal Classic*, which was composed more than 2000 a long time prior. The charcoal prepared product of ASA, ASAC Carbonisata (ASAC), has long been utilized for its anti-inflammatory impacts. However, the material basis and mechanism of action of ASAC stay vague.

In this study, novel CDs (named ASAC-CDs) were prepared by green and one-step calcination strategy utilizing ASAC as sole carbon sources, and the physicochemical properties of ASAC-CDs including morphology, optical properties were characterized by a series of strategies, basically including electron microscopy, optical instrument. In addition, the anti-inflammatory impact of ASAC-CDs on ALI actuated by LPS in rats has been considered for the primary time.

Materials and Methods

Chemicals

ASA was obtained from Beijing Qian Baicao Co., Ltd (Beijing, China), and ASAC was prepared in our research facility. Analytical-grade chemical reagents were obtained from Sinopharm Chemical Reagents Beijing (Beijing, China). Dialysis membranes (molecular weight cut off was 1000 Da) were brought from Beijing Ruida Henghui Innovation Improvement Co., Ltd (Beijing, China). Cell

counting kit-8 (CCK-8) was gotten from Dojindo Atomic Advances, Inc., (Kumamoto, Japan). All the tests were performed utilizing deionised water (DW).

Animals

All the experimental procedures were performed in agreement with the Regulations for the Administration of Affairs Concerning Experimental Animals approved by the State Council of People's Republic of China. The animal experimental design and protocols used in this study were approved by the Ethics Review Committee for Animal Experimentation at the Beijing University of Chinese Medicine. Adenocarcinoma human alveolar basal epithelial cells (A549) were acquired with Peking Union Cell Bank (Beijing, China). Male grown-up Sprague–Dawley (SD) rats (weighing 250.0 ± 10.0 g) were acquired from Beijing Jinmuyang Risk Co., Ltd. (Beijing, China) and kept in a well-ventilated room at 24.0 ± 1.0°C with 55–65% relative humidity and a 12 h light:dark cycle. The animals were given water and nourishment advertisement libitum.

Preparation of PARC-CDs

To begin with, 170 g ASA was set in crucibles, secured with aluminum foil paper and the top was closed to make a tight seal, at that point calcined in a muffle furnace (TL0612, Beijing Zhong Ke Anbo Innovation Co., Ltd., China) for 1 h at 300°C to deliver ASAC and cooled to room temperature. The ASAC was pulverized into an oil solution with a pulverizer, and extracted with 1400 mL of deionized water for 2 hours, repeated three times, and the obtained aqueous solutions were combined. After filtering the residue with filter paper, the solution was concentrated in 100 mL and then dialyzed utilizing a 1.0 kDa dialysis membrane for 72 hours. At long last, the water extraction containing ASAC-CDs was put away at 4°C until further experimentation. The schematic chart of the experimental protocol is portrayed in Figure 1.

Fingerprint Analysis of ASAC-CDs

The components of the aqueous ASAC solution obtained at 300°C and the methanol ASA extract were measured utilizing an Agilent 1260 series high-performance liquid chromatography (HPLC) instrument (Agilent, Waldbronn, Germany). A C18 column (250 mm × 4.6 mm, Orochem, IL, USA) packed with 5 mm octadecyl-bonded silica (C18) was utilized for ASAC-CDs separation. All samples were filtered with a 0.22 μm cellulose membrane (Jin Teng, Tianjin, China) prior to use. The mobile phases A and B were 0.1% phosphoric acid solution and acetonitrile, respectively. As previously reported,[16] a modified isocratic elution program was performed at a flow rate of 1.0 mL/min as follows: 0–50 min, 8% A, 92% B. The column temperature was 25°C and the injected sample

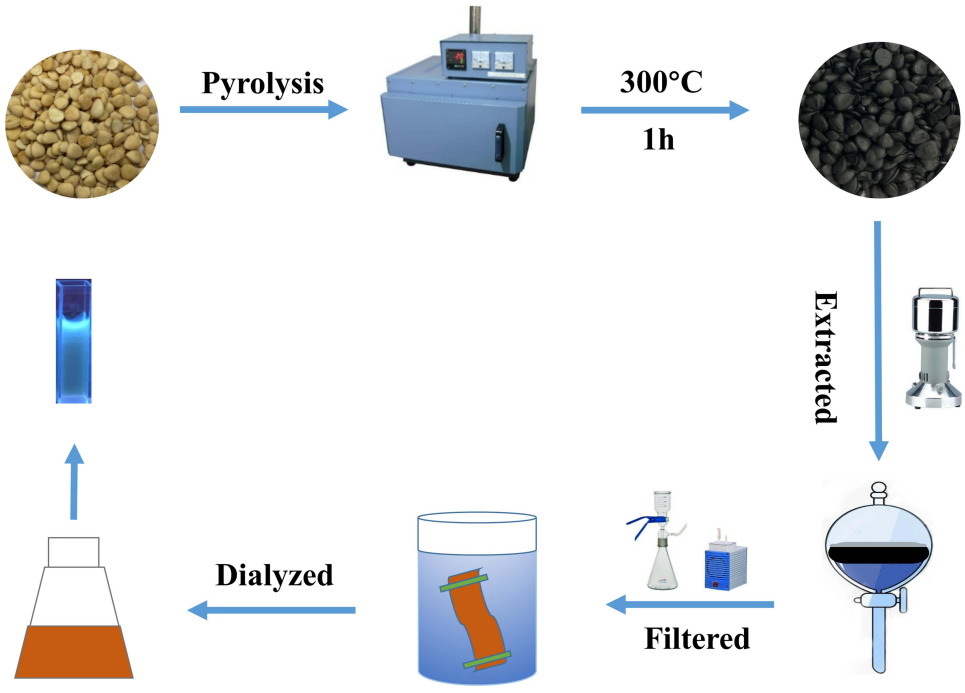

Figure 1 The flowchart for the preparation process of ASAC-CDs.

quantity maintained at 10 μL. The detection wavelength was set at 207 nm.

Characterisation of ASAC-CDs

The morphology, particle size distribution and microstructure of ASAC-CDs were characterized by TEM (Tecnai G220; FEI Company, USA) at an accelerating voltage of 100 kV. Atomic lattice fringes and other structural details were observed by HRTEM (JEN-1230; Japan Electron Optics Laboratory; Japan). The fluorescent performances and ultraviolet-visible (UV-vis) absorption spectra of the CDs were analysed using ultraviolet spectrophotometer (CECIL, Cambridge, UK) and fluorescence spectrophotometer (F-4500, Tokyo, Japan). XRD (D8-Advanced X-ray diffractometer, Bruker AXS, Karlsruhe, Germany) was performed with Cu K-alpha radiation. Fourier transform infrared (FTIR) spectroscopy (Thermo, California, USA) was utilized to recognize the composition of functional groups on the surface of ASAC-CDs from 400 to 4000 cm^{-1}. In addition, the surface and elemental compositions of ASAC-CDs were further observed utilizing X-ray photoelectron spectroscopy (XPS) (ESCALAB 250Xi; Thermo Fisher Scientific, USA) with a mono X-ray source Al Kα excitation (1486.6 eV). A freezing centrifuge (TGL-16G) was obtained from Beijing Restorative Centrifuge Manufacturing plant (Beijing, China).

Quantum Yield of ASAC-CDs

Quantum yield (QY) was measured with quinine sulfate as the reference (%QY was 54 in 0.1 M sulphuric acid [H_2SO_4] solution).[17,18] In an arrangement to play down the reabsorption impact, A_C and A_R were ensured underneath 0.05. QY of the ASAC-CDs is calculated concurring to the following equation.

$$QY_{CDs} = QY_R I_{CDs} A_R \eta_{CDs}^2 / (I_R A_{CDs} \eta_R^2)$$

where QY represents fluorescence quantum yield, I is the measured integrated emission intensity, A and η represent the 353 nm absorption value and the refractive index of the solvent. "CDs" and "R" represent the ASAC-CDs and the standard, respectively.

Cell Viability Assay

Security is one of the primary components to be considered in clinical applications.[19] A549 cells were utilized to assess the potential cytotoxicity of ASAC-CDs using a CCK-8 assay. The A549 cells were cultured in McCoy's 5A supplemented with 20% fetal bovine serum at 37°C in a humidified 5% CO_2 atmosphere. Firstly, the cells were spread on a 96-well plate at a density of 1×10^5 per well for 24 hours. Then, the cells were treated with various concentrations (1000, 500, 250, 125, 62.5, 31.25, 15.63, 7.81, 3.91 μg/mL, 100 μL/well) of ASAC-CDs in serum-free media, followed by incubation for another 24 h. After the plate was cleaned three times with PBS, 10 μL of CCK-8 reagent was added to each well for an additional 4h incubation. A microplate reader (Biotek, Vermont, USA) was used to measure the absorbance of each well at 450 nm. The cell viability was calculated according to the following formula:

$$\text{Cell Viability (\% of control)} = \frac{Ae - Ab}{Ac - Ab} \times 100$$

where Ae, Ab and Ac represent the absorbance of the experimental, blank and control groups, respectively, at 450 nm.

Models of ALI and Drug Treatment

The ALI model was established as previously reported.[20] Male SD rats were randomized into the following six groups (n = 8 in each) and treated as indicated: the negative control group (normal saline [NS] intraperitoneal injection), the model group (intraperitoneal injection), the positive control group (5 mg/kg [Dexamethasone] intraperitoneal injection) and the high-, medium- and low-dose ASAC-CDs groups (3.75, 1.88 and 0.94 mg/kg, respectively, intraperitoneal injection). The normal group and the model group were given equal volumes of normal saline, and all the ASAC-CDs groups underwent intraperitoneal administration for 10 days. 1 hour after the final administration, all the groups were injected intraperitoneally with the prepared lipopolysaccharides solution (5 mg/kg), except for the negative control group, which received an intraperitoneal injection of an equal volume of normal saline.

Detection of Cytokines in Serum

After eight hours, rats were anaesthetized with 4% chloral hydrate (0.40 g/kg). Blood samples were collected from rats via the abdominal aorta by blood taking needles (Shandong Junnuo co., Ltd, Heze, China) and vacuum blood collection tubes (Becton Dickinson Medical Instrument co., Ltd, Shanghai, China). Blood samples were maintained at room temperature for 60 min, after

which serum was separated from whole blood by centrifugation at 750× g for 15 min at 4°C. The levels of IL-6, IL-1β, TNF-α and IL-10 in serum from rats were determined by ELISA (Cloud-Clone Crop Technology co., Ltd., Wuhan, China), following the manufacturer's instructions.

Histopathological Study

The SD rat left lung tissue samples were fixed in 10% neutral-buffered formalin at 4°C for more than 48 h, dehydrated, embedded in paraffin, cut into sections, and then stained with haematoxylin and eosin (H&E). Morphological changes were compared among the control group, model group, positive drug group and the high-, medium- and low-dose ASAC-CDs groups were compared. At the same time, according to the previously reported method,[21] 50-fold light microscope was used to observe the three examination items of pulmonary edema, alveolar and interstitial inflammatory cell infiltration, and interstitial hemorrhage formation in the double-blind state. Subjective quantitative score of 0–4 points was respectively conducted: 0 points for no lesion of the specimen, 4 points for full field of vision, and the pathological score was the sum of the above items.

Measurement of Myeloperoxidase Activity and Antioxidant Levels

The right lungs of the mice were removed, rapidly frozen in dry ice and stored at −80°C until use in the following procedures. Tissue samples (100 mg) from the different groups were homogenized with PBS on ice and then centrifuged at 750×g for 15 min. The supernatants were collected to determine levels of MPO, MDA, SOD and GSH using respective kits according to the manufacturer's instructions.

Statistical Analysis

The statistical analysis was carried out using the computer programme SPSS (version 19.0, Chicago, IL). The non-normally distributed data were expressed as the median (quartile range). The normally distributed data and homogeneous variances were expressed as the mean ± standard deviation. Multiple comparisons were performed using one-way analysis of variance (ANOVA) followed by least significant difference test. $p < 0.05$ and $p < 0.01$ indicated statistically significant differences.

Results

High-Performance Liquid Chromatography Data Analysis

It can be observed from Figure 2A that the chromatogram of methanol extract of ASA is complex and that there are many types of small molecules. The specific peak of amygdalin, an index component, can be clearly seen. As appeared in Figure 2B, no significant peaks were observed in the ASAC-CDs solution under the same liquid phase conditions. Through the observation and comparison of HPLC, the interference of small molecule compounds was removed to a certain extent.[22]

Characterization of ASAC-CDs

The TEM image of the ASAC-CDs uncovered that the CDs were about spherical and isolated from each other without clear accumulation (Figure 3A). The particle size distribution of SRC-CDs is primarily distributed between 1.5 and 5.5 nm (Figure 3B), which is in line with the normal distribution characteristics.[23] This is often the conclusion drawn by the factual examination of more than 100 particles utilizing ImageJ computer program. As shown in Figure 3C, the HRTEM image showed well-resolved lattice fringes and a lattice spacing of 0.215 nm. These morphological extents were reliable with past research reports.[24] Figure 3D shows that the XRD spectrum of ASAC-CDs had distinct diffraction peaks ($2\theta = 20.835°$), indicating that ASAC-CDs were attributed to amorphous carbons arranged in a considerably random fashion and its atomic lattice fringes were calculated at 0.426 nm utilizing MDI Jade 6 software.[25]

The luminescent properties of the ASAC-CDs were examined following. The UV-Vis spectrum (Figure 3E) of the aqueous ASAC-CDs solution exhibited a small absorption peak at 260 nm, which was ascribed to the π–π* electron transition of the conjugated C=C bonds and aromatic sp^2 domains.[26] The fluorescence emission spectra showed a highest emission peak at 436 nm when excited at 353 nm in Figure 3F, and the QY of ASAC-CDs was calculated to be 3.17% utilizing quinine sulphate as a reference. As shown in Figure 3G, with the increase of excitation wavelength from 300 nm to 380 nm, the maximum emission wavelength of ASAC-CDs had a red shift and its fluorescence intensity also showed a trend of first increasing and then decreasing. The surface chemical characteristics of the ASAC-CDs were analyzed by FTIR spectroscopy (Figure 3H). The strong characteristic absorption at 3444 cm^{-1} indicated

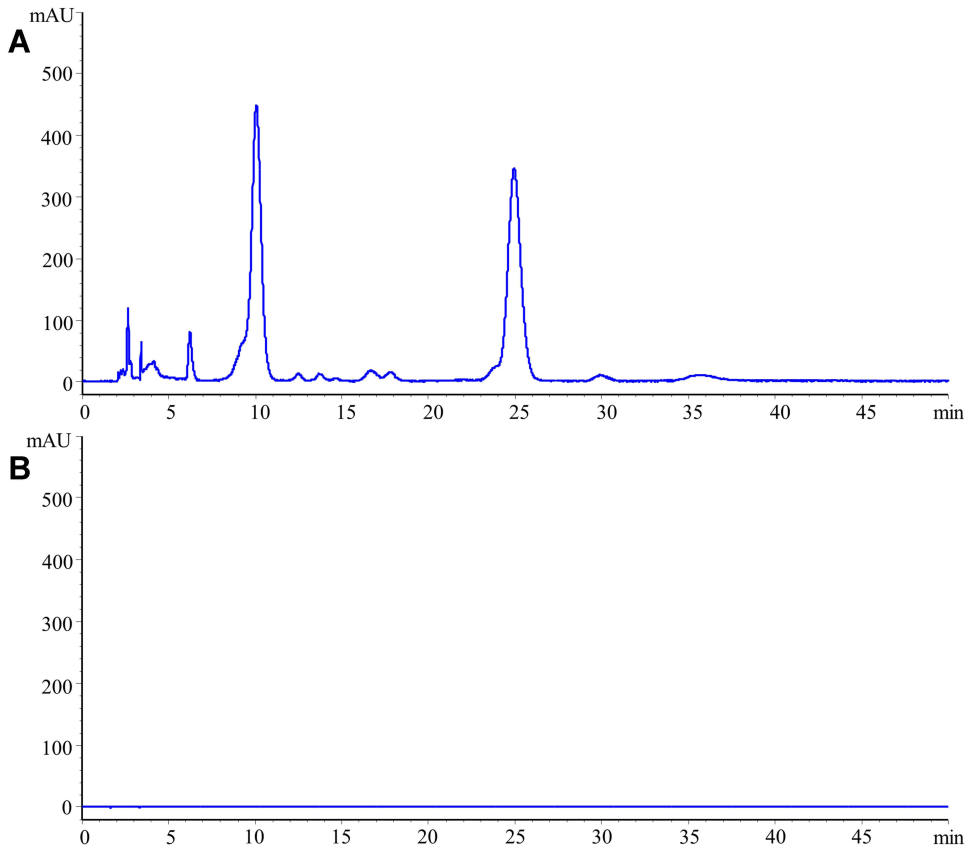

Figure 2 High-performance liquid chromatography (HPLC) fingerprint of (**A**) ASA (the dry mature seeds of *Prunus armeniaca L.*) and (**B**) *Armeniacae Semen Amarum Carbonisata.*

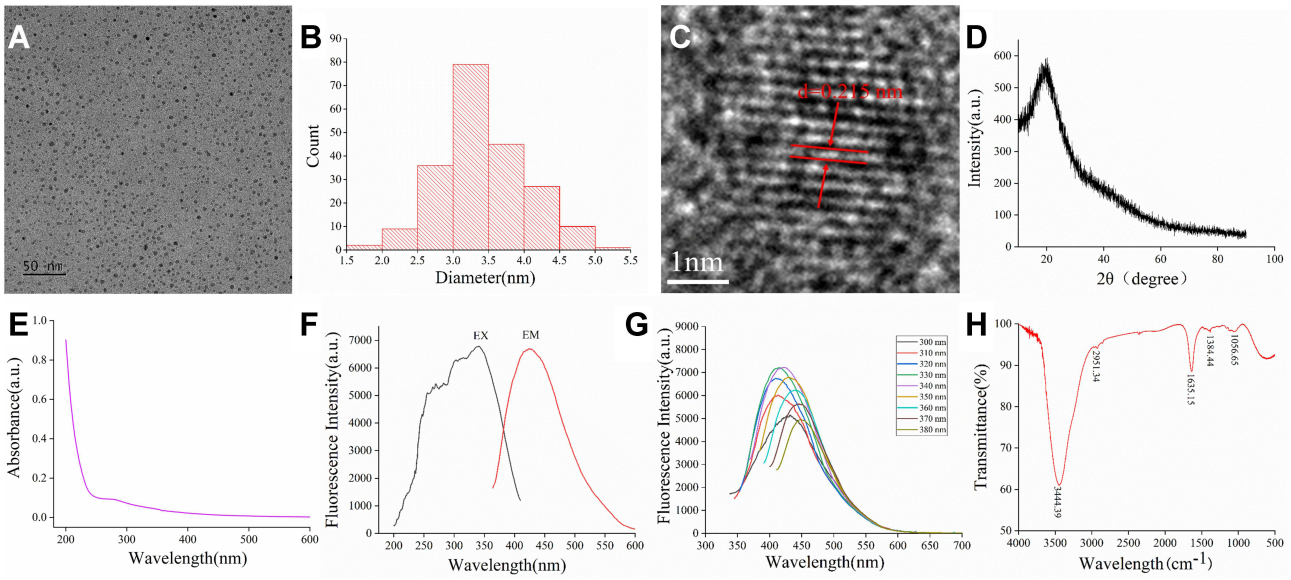

Figure 3 Characterization of ASAC-CDs: (**A**) Transmission electron microscopy (TEM) images of ASAC-CDs displaying ultra-small particles. (**B**) Particle size distribution histogram of ASAC-CDs. (**C**) High-resolution TEM image of ASAC-CDs and lattice spacing of ASAC-CDs (in the middle). (**D**) X-ray diffraction pattern. (**E**) Ultraviolet–visible spectrum. (**F**) Fluorescence spectra for excitation and emission. (**G**) Fluorescence spectra of ASAC-CDs with different excitation wavelengths. (**H**) Fourier transform infra-red spectrum.

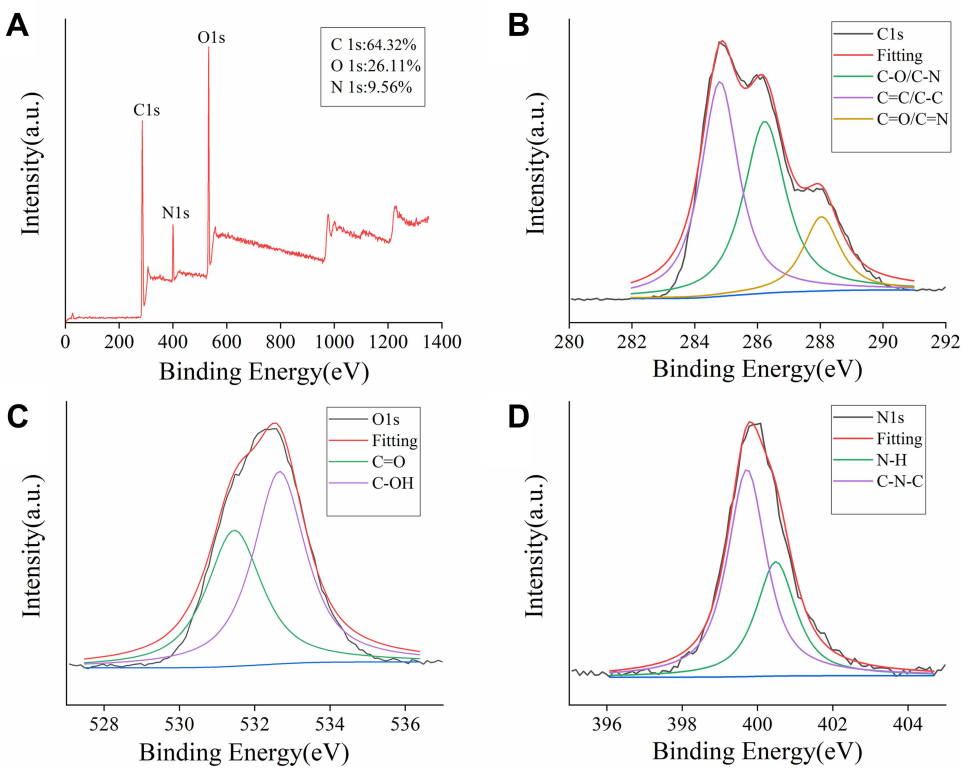

Figure 4 The surface composition and elemental analysis of the prepared ASAC-CDs by XPS. (**A**) X-ray photoelectron spectroscopy survey of ASAC-CDs. (**B**) C1s. (**C**) O1s and (**D**) N1s.

the existence of -O-H stretching vibration. The absorption signals at 2951 cm^{-1} and 2867 cm^{-1} were attributed to -C-H stretching, which may occur because of the association of methyl or methylene groups with the aliphatic hydrocarbons present in ASAC-CDs. The intense peak at about 1635 cm^{-1} was identified as C=O. The peak at 1384 cm^{-1} was attributed to the stretching vibration peak of C-N. In addition, the peak at 1056 cm^{-1} was related to C-O-C bonds.[27] The presence of these functional groups, including carbonyl, carboxyl, hydroxyl, confers hydrophilicity and aqueous solubility on ASAC-CDs.[15]

The element composition and surface functional group situations of the ASAC-CDs were encouraged to be examined by XPS. As shown in Figure 4A, peaks were evident at 285.16, 399.92 and 532.28 eV, indicating that the CDs were composed primarily of C (64.32%), O (26.11%), and a small amount of N (9.56%). The C1s spectrum (Figure 4B) was divided into three peaks at 284.80, 286.23, and 288.04 eV, which were consistent with C=C/C-C, C-O/C-N and C=O/C=N bonds. The O1s spectrum (Figure 4C) was separated into two peaks at 531.46 and 532.66 eV, which were assigned to C–O and C=O, respectively. Furthermore, Figure 4D appears the N1s spectrum, demonstrating the distinctive chemical situations of C-N-C at 399.72 eV and N-H at 400.49 eV.[28,29] These come about were steady with the surface composition of ASAC-CDs decided by the FTIR examination.[30]

Cytotoxicity Detection

The security of carbon dots has continuously been a vital issue in natural applications. In an arrangement to consider the harmfulness of ASAC-CDs and investigate its security, the CCK-8 test was carried out to distinguish the cytotoxicity of ASAC-CDs to A549 cells. As shown in Figure 5, the viabilities of A549 cells treated with ASAC-CDs in the concentration range from 3.91 to 1000 μg/mL for 24 h. ASAC-CDs showed an inhibitory effect on cell proliferation when the concentration of ASAC-CDs was 31.25 ~ 1000 μg/mL ($P < 0.01$), and the inhibitory effect showed a weakening trend as the concentration decreased. After the concentration drops to 15.63 μg/mL, ASAC-CDs can promote proliferation to a certain extent. However, ASAC-CDs had almost no effect on cell proliferation when the dosage was reduced to 7.81 μg/mL. This has a certain

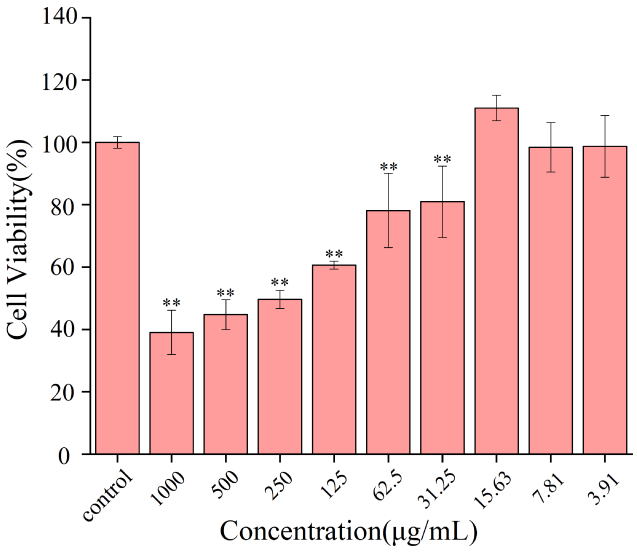

Figure 5 Effect of different concentrations of ASAC-CDs on the viability of A549 cells. Significantly different compared to the control group at **p < 0.01.

potential reference value for future research and development of drugs to enhance target cell viability.

The ASAC-CDs Mitigated LPS-Induced Acute Lung Injury in Rats

This study explored the protective effect of ASAC-CDs on LPS-induced acute lung injury in rats. The main pathological features of acute lung injury are inflammatory cell infiltration, massive production of inflammatory mediators, and diffuse pulmonary inflammation. Compared with the control group (Figure 6A), the lungs of rats injected with LPS in the intraperitoneal cavity showed extensive thick and dark red hemorrhages, indicating that the lungs have severe inflammatory lesions (Figure 6B). In contrast to the model group rats, animals treated with dexamethasone (Figure 6C) and ASAC-CDs (Figure 6D–F) displayed lighter and smaller hemorrhages, which showed less harm and severity in those groups.

Histopathological changes in lung tissues in lipopolysaccharides-induced ALI rats were further evaluated. As shown in Figure 7Ai, the lung tissue structure of the rats in the control group was normal and the alveolar compartment was slender. No obvious inflammatory cell infiltration was observed in the alveolar cavity. From the model group (Figure 7Aii), it can be clearly seen that inflammatory cells and red blood cells penetrated the alveolar cavity and lung interstitium, the shape of the alveoli changed, and the structural integrity of the alveoli was destroyed, indicating the success of the preparation of the ALI model. In contrast, pretreatment with dexamethasone (Figure 7Aiii) and the high-dose ASAC-CDs (Figure 7Aiv) significantly ameliorated the infiltration state of inflammatory cells and red blood cells in the alveolar cavity and lung interstitium. Additionally, various degrees of reduction in inflammatory

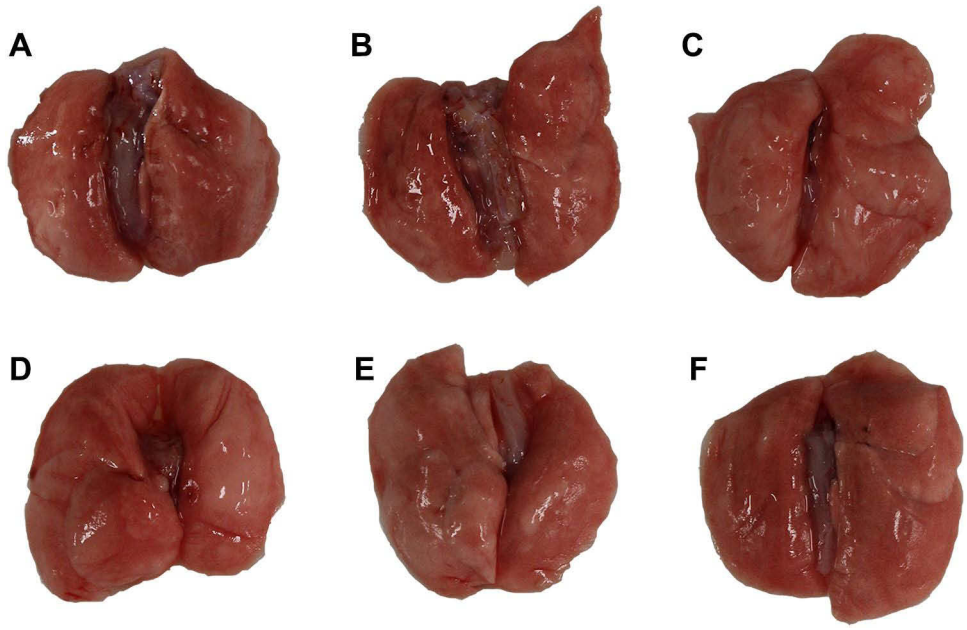

Figure 6 Macroscopic images of ASAC-CDs ameliorating an LPS-induced acute lung injury (ALI) in rats. (**A**) Normal saline group; (**B**) model group; (**C**) positive control group; (**D**) high-dose ASAC-CDs group; (**E**) medium-dose ASAC-CDs group; and (**F**) low-dose ASAC-CDs group.

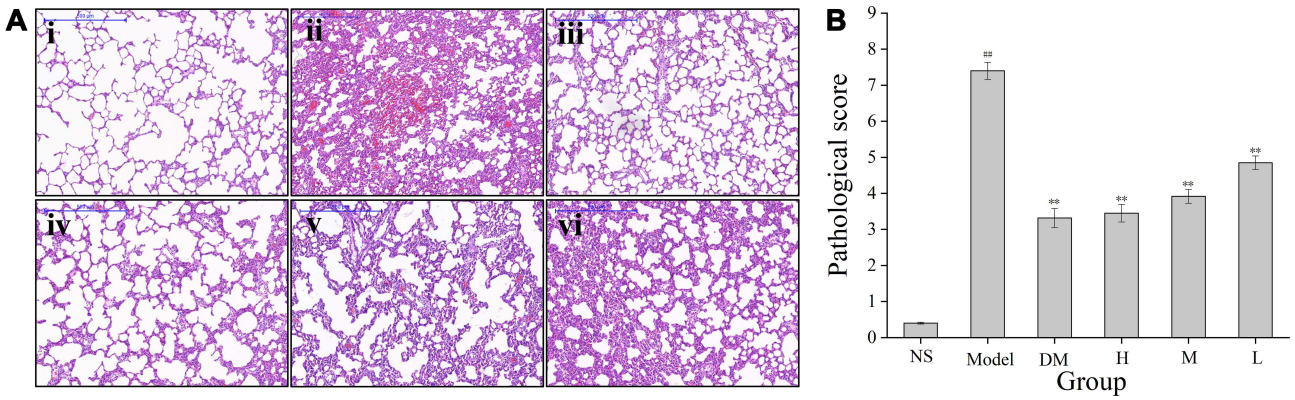

Figure 7 ASAC-CDs ameliorate LPS-induced lung histopathological damage. (**A**) Effects of ASAC-CDs on histopathological changes in lung tissues in LPS-induced ALI rats (magnification=50 x). Histopathological sections of lung tissue were stained with H&E. (i) normal saline group; (ii) model group; (iii) positive control group; (iv) high-dose ASAC-CDs group; (v) medium-dose ASAC-CDs group; and (vi) low-dose ASAC-CDs group. (**B**) Pathological score of the ALI model induced with LPS in rats treated with normal saline (NS), LPS (Model), dexamethasone (DM), and high (H), medium (M), and low (L) doses of ASAC-CDs (3.75, 1.88 and 0.94 mg/kg, respectively). Significantly different compared with the control group at $^{\#\#}p < 0.01$, significantly different compared to the model group at $^{**}p < 0.01$.

cell in the medium- and low-dose groups of ASAC-CDs (Figure 7Av and vi) can be observed, suggesting that there may be a certain dose-effect relationship.

As can be seen from Figure 7B, compared with the control group, the pathological score of lung tissue in the model group was significantly higher ($P < 0.01$). Compared with the model group, the pathological scores of lung tissues in the high-, medium- and low-dose groups and dexamethasone groups were significantly decreased in a dose-dependent manner ($P < 0.01$).

Effect of ASAC-CDs on Inflammatory Cytokines in Serum

IL-6, IL-1β, TNF-α and IL-10 are important inflammatory factors in acute inflammation, as shown in Figure 8A, compared with those in the control group (2.55 ± 0.26 pg/mL), the serum concentrations of IL-6 in the model group (20.56 ± 1.41 pg/mL) were significantly elevated ($P < 0.01$), indicating that the model was functional. Compared with those in the model group, the serum concentrations of IL-6 in the dexamethasone group (6.97 ± 1.60 pg/mL), high- and medium-dose ASAC-CDs groups (8.13 ± 1.40 pg/mL, 8.93 ± 1.89 pg/mL, respectively) was significantly reduced ($P < 0.01$), and that in the low-dose ASAC-CDs groups (13.14 ±1.22 pg/mL) was decreased ($P < 0.05$).

Similarly, compared with those in the control group (4.35 ± 0.58 pg/mL), the concentrations of IL-1β (Figure 8B) in the model group (21.07 ± 2.26 pg/mL) also increased ($p < 0.01$). Compared with those in the model group, the serum concentrations of IL-1β in the dexamethasone group (9.47 ± 0.70 pg/mL) and high-dose ASAC-CDs groups (8.53 ± 0.82 pg/mL) were significantly lower ($P < 0.01$), and that in the medium and low-dose ASAC-CDs groups (15.34 ±1.37 pg/mL, 15.41 ±1.27 pg/mL) was decreased ($P < 0.05$).

Additionally, compared with those in the control group (23.46 ± 1.47 pg/mL), the levels of TNF-α (Figure 8C) in the model group (69.49 ± 9.62 pg/mL) significantly increased ($p < 0.01$). Compared with the levels in the model group, the dexamethasone group (28.13 ± 3.16 pg/mL) showed significantly reduced inflammation. The levels of TNF-α were decreased more obviously following treatment with high and medium doses ASAC-CDs to 32.03 ± 5.20 and 36.40 ± 5.63 pg/mL, respectively ($p < 0.01$), the results of the low-dose group showed no statistical significance.

The IL-10 level in the serum of the model group (92.47 ± 10.92 pg/mL) increased irritability ($p < 0.01$) in comparison to that of the control group (51.04 ± 8.12 pg/mL). Similarly, the level of IL-10 in the positive (150.59 ± 17.95 pg/mL; $p < 0.01$), high-dose (134.33 ± 9.92 pg/mL; $p < 0.01$), medium-dose (123.43 ± 16.59 pg/mL; $p < 0.01$) and low-dose (109.94 ± 13.97 pg/mL; $p < 0.05$) groups produced a significant increase compared with that in the model group (Figure 8D).

Effect of ASAC-CDs on Myeloperoxidase Activity and Antioxidant Levels

Oxidative stress is one of the important mechanisms for the occurrence and development of inflammation in ALI. Severe oxidative damage was triggered by reactive oxygen

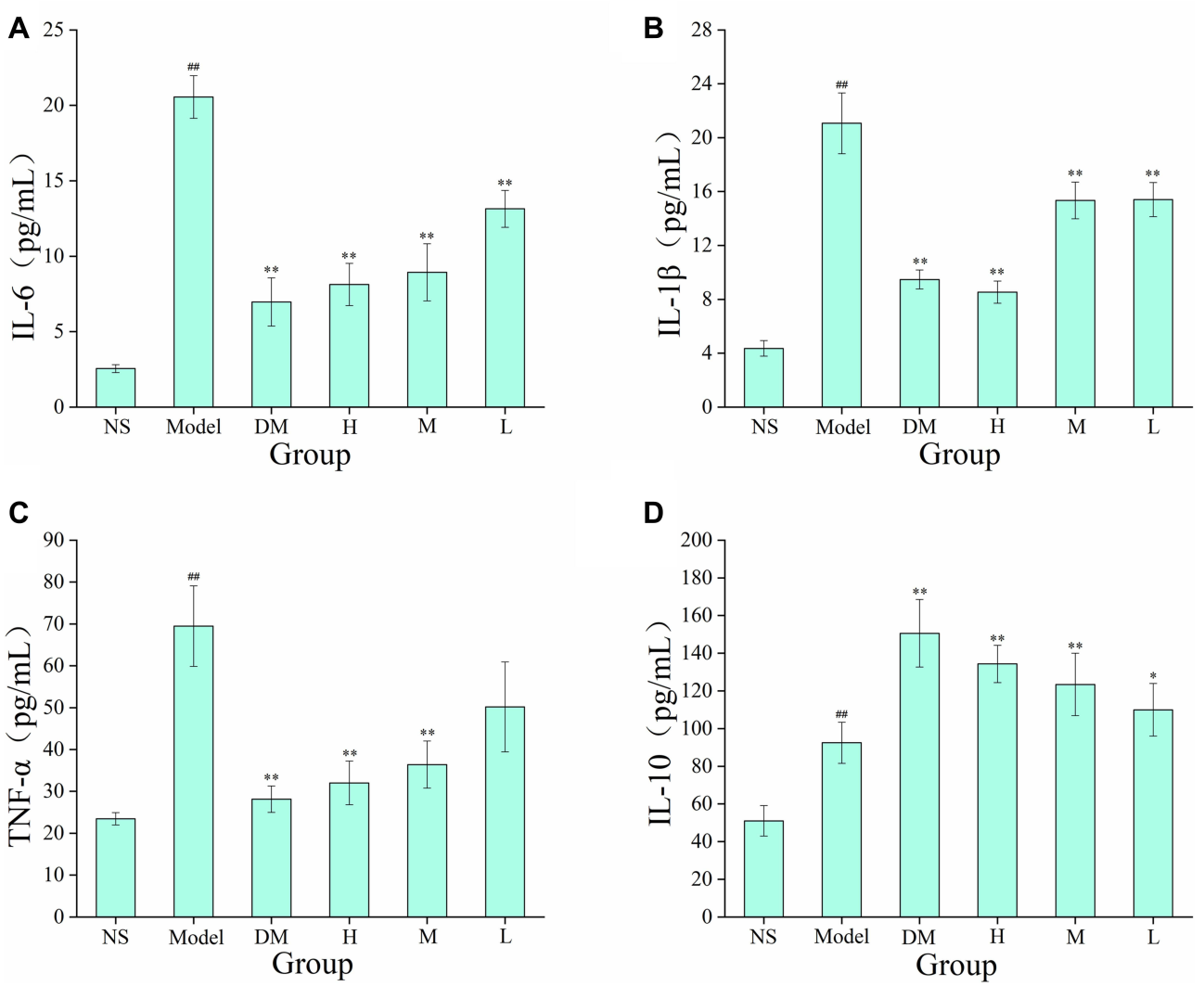

Figure 8 Serum concentrations of (**A**) IL-6, (**B**) IL-1β, (**C**) TNF-α and (**D**) IL-10 in rats treated with normal saline (NS), LPS (Model), dexamethasone (DM), and high (H), medium (M), and low (L) doses of ASAC-CDs (3.75, 1.88 and 0.94 mg/kg, respectively). Significantly different compared with the control group at $^{\#\#}p < 0.01$, significantly different compared to the model group at $^{**}p < 0.01$ and $^{*}p < 0.05$.

species and played a vital role in inflammation and hemorrhage lesions. The redox state changes are further characterized by evaluating the inflammation state (MPO) and antioxidant levels (MDA, SOD, GSH) in the lung tissues (Figure 9A–D).

LPS of the model group caused significant increase in the activities of MPO (1.13 ± 0.05 U/g, $p < 0.01$) and the levels of MDA (6.29 ± 0.22 nmol/mg port, $p < 0.01$) compared with the control group (MPO: 0.60 ± 0.05 U/g; 3.88 ± 0.17 nmol/mg port). Meanwhile, compared with the control group (SOD: 154.14 ± 15.69 U/mg prot; GSH: 6.46 ± 0.92 μmol/g prot), LPS of the model group caused significant decrease in the activities of SOD (71.99 ± 9.15 U/mg prot) and GSH (3.91 ± 0.26 μmol/g prot).

In addition, as compared to model group, the levels of MPO and MDA in the dexamethasone group (MPO: 0.77 ± 0.08 U/g; MDA: 4.66 ± 0.27 nmol/mg port) and high- (MPO: 0.80 ± 0.06 U/g; MDA: 4.81 ± 0.34 nmol/mg port), medium- (MPO: 0.83 ± 0.09 U/g; MDA: 4.95 ± 0.33 nmol/mg port) and low-dose (MPO: 0.87 ± 0.04 U/g; MDA: 5.02 ± 0.12 nmol/mg port) ASAC-CDs groups were significantly reduced ($P < 0.01$). What is more, in comparison to the control group, the improvement of those antioxidants was more obvious in the dexamethasone group (SOD: 134.93 ± 11.62 U/mg prot; GSH: 5.67 ± 0.34 μmol/g prot, $p < 0.01$) and high-dose ASAC-CDs group (SOD: 127.59 ± 15.72 U/mg prot; GSH: 5.61 ± 0.22 μmol/g prot, $p < 0.01$). In contrast to the model group, the medium-dose of ASAC-CDs could significantly

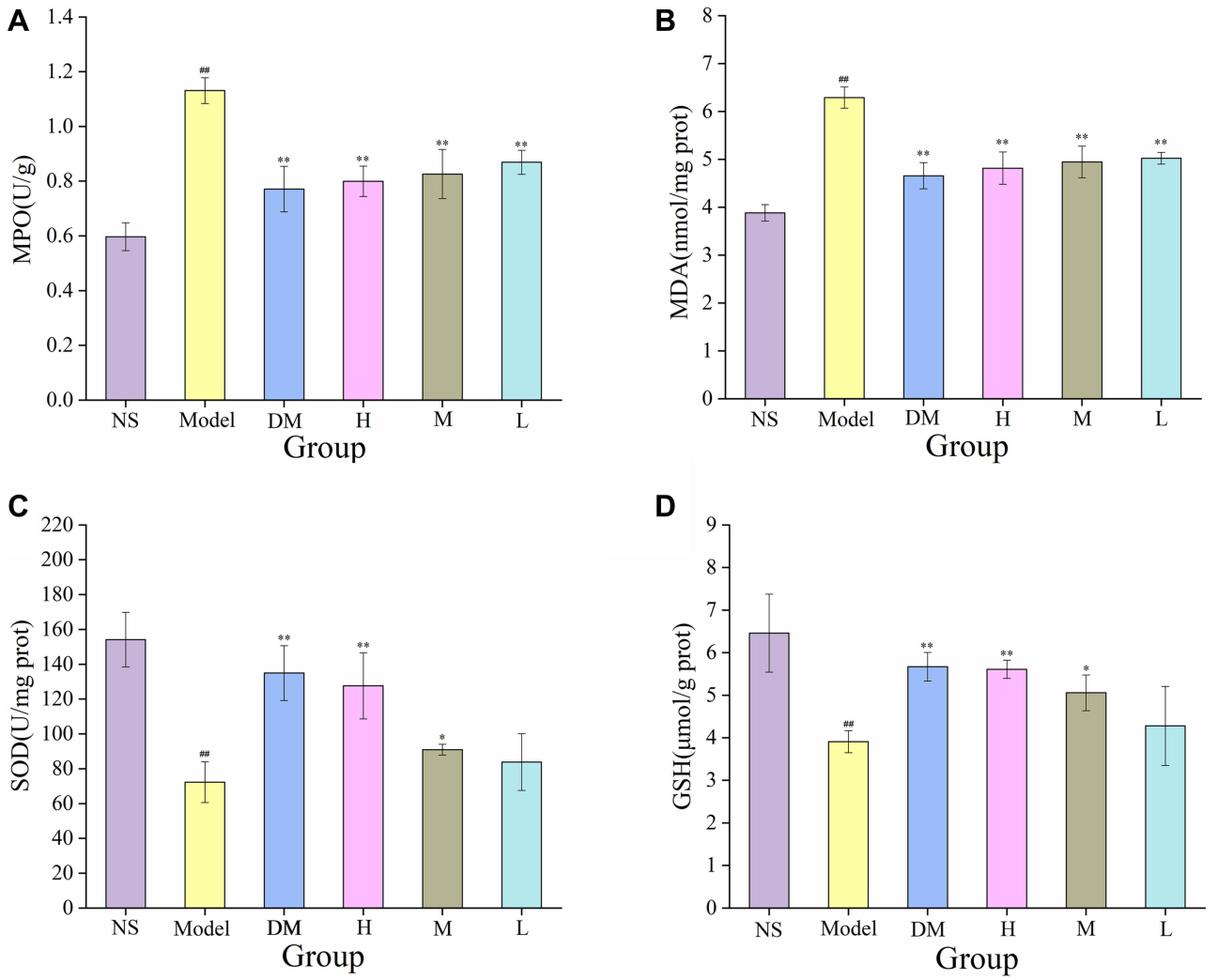

Figure 9 Effects of myeloperoxidase activity and antioxidant levels in the lung tissue. (**A**) MPO, (**B**) MDA, (**C**) SOD and (**D**) GSH levels in rats treated with normal saline (NS), LPS (Model), dexamethasone (DM), and high (H), medium (M), and low (L) doses of ASAC-CDs (3.75, 1.88 and 0.94 mg/kg, respectively). Significantly different compared with the control group at $^{\#\#}p < 0.01$, significantly different compared to the model group at $^{**}p < 0.01$ and $^{*}p < 0.05$.

up-regulate the activities of SOD (90.90 ± 3.12 U/mg prot, $p < 0.05$) and GSH (5.06 ± 0.42 μmol/g prot, $p < 0.05$). Compared with those in the model group, there was no significant difference observed in the low-dose ASAC-CDs group.

Discussion

Charcoal drugs are a kind of processed product utilized in TCM with special properties conferred by high-temperature carbonization, which produces CDs. Through preparatory work, our investigation group has demonstrated that CDs are the material basis for the activity of charcoal drugs. We have reported that the carbonisata-derived CDs of charcoal drugs such as *Junci Medulla*[31] have remarkable anti-haemorrhage effects and CDs derived from *Crinis Carbonisatus*[32] perform neuroprotective effect on cerebral ischemia and reperfusion injury. In addition, *Aurantii fructus immaturus*[14] carbonisata-derived carbon dots have anti-hyperuricaemic and anti-gouty arthritis activity, which can diminish serum uric acid by restraining xanthine oxidase activity in hyperuricaemic rats and in vitro. What's more interesting is that CDs prepared with the *Phellodendri Chinensis* as a precursor not only have a remarkable protective effect on deinagkistrodon acutus venom-induced acute kidney injury, but also can ameliorate imiquimod-induced psoriasis-like inflammation in mice by regulating of M1/M2 macrophage polarization.[10,33] Just as indications for examining artemisinin were found in ancient Chinese pharmaceutical books, clues were gotten from antiquated archives, and comparable handling strategies were utilized

to get ASAC-CDs extricated from ASAC to study its efficacy.

Nanomaterials have attracted large-scale medical research due to their unique nanosheet structure, large surface area and excellent physical and chemical properties. To begin with, in terms of physical work, nanoparticle protein crowns demonstrate a physical adsorption function.[34] Proteins bind to nanoparticles to form a protein corona, fundamentally altering the nanoparticles' biological capacity in biological fluids.[35] In terms of chemical and biological function,[36] nanomaterials are related with an assortment of active groups, which may tie to receptors or proteins. These properties are the material basis for nanomaterials' functions. As the carbon-based nanomaterial latest joining the carbon family, CDs got colossal considerations with the nonstop investigation by various researchers.[37] The one of a kind advantage[38,39] prompted scientists focus on the inherent activity of CDs, but related study is still in its infancy. Abundant underlying bioactivities were not investigated and found up to now, which deterred the further applications of CDs in science, especially in vivo. Against this status quo, CDs with novel bioactivity were merited to be created to advance broaden their application in bioactive areas.

In this study, novel CDs were found and isolated from the ASAC watery extract and distinguished as ASAC-CDs utilizing advanced spectroscopy instrument. HPLC was used to compare the chemical composition differences between ASA and ASAC-CDs. The main effective components of ASA include amygdalin. In contrast, there were no small molecule compounds in ASAC-CDs obtained after high-temperature carbonization and filter dialysis, which removed the influence of small molecule substance on biological activity to a certain extent, thus determining the biological activity of ASAC-CDs. Our experimental results indicated that we removed the small molecule compounds from the original drug. In addition, under the temperature condition of 18.4°C, the PH value of the ASAC-NCs solution with a concentration of 0.5 mg/mL is 7.49, which is almost a neutral solution.

Herein, we found that the ASAC-CDs seem to decrease the level of inflammatory factors. Histological observations and changes in cytokine discovery data unequivocally bolster this result. Overexpression of inflammatory cytokines is one of the signs of inflammatory reaction. The blood picture of acute inflammatory reaction is primarily characterized by lifted neutrophils.[40] Beneath the activity of LPS incitement, neutrophils quickly invade lung tissue, causing related inflammatory cells to be actuated and discharge an arrangement of inflammatory factors,[41] such as IL-6, IL-1β and TNF-α. As an anti-inflammatory factor, IL-10 has a protective effect on the body during inflammation, which can inhibit the development of inflammatory response and avoid unnecessary tissue damage caused by inflammatory factors.[42] It appears that, compared with the model group, the ASAC-CDs group can decrease the levels of IL-6, IL-1β and TNF-α and increase the contents of IL-10 in rat serum to shifting degrees, particularly the high-dose group. This shows that ASAC-CDs can decrease the increment of neutrophils within the blood to a certain degree, diminish the chemotaxis of neutrophils to inflammatory sites, subsequently lessening the discharge of inflammatory mediators, and restraining lung tissue harm and aggravation actuated by LPS.

The aggregation of neutrophils is a key link in the pulmonary inflammation. MPO is the function and actuation stamp of neutrophils, and its activity level can by implication reflect the degree of conglomeration of neutrophils in inflammation sites.[43] MDA is the oxidation product of oxygen-free radicals acting on lipids, and its content increments altogether with the devastation of membrane structure and function.[44] SOD and GSH are vital antioxidant active substances within the body, which can diminish the generation of free radicals in intense inflammation.[45] Oxidative stress is oxidative harm intervened by overexpression of responsive oxygen species, and is another key mechanism of LPS-induced ALI.[46] MPO, MDA, SOD, and GSH are vital indicators that reflect the level of oxidative stress in lung tissue.[47,48] From the comes about, on the one hand, it moreover appears that ASAC-CDs can diminish the content of MDA and MPO in rat lung tissue, demonstrating that ASAC-CDs can diminish the harm of inflammation to the lungs by improving the antioxidant impact. On the other hand, ASAC-CDs can increment the activity of SOD and the content of GSH in rat lung tissue to a certain degree, which moreover suggests the antioxidant activity of ASAC-CDs.

Synthesized by means of a green strategy with a broad antecedent source, ASAC-CDs not only show a helpful impact, but also appear to have no obvious biological toxicity and have exceptional biocompatibility, which show that they have colossal potential as a candidate treatment for ALI. The results of this study indicate that ASAC-CDs incorporate a certain defensive impact on LPS-induced ALI, and its preliminary mechanism may be related to its antioxidant activity, diminishment of respiratory edema and hindrance of inflammation. This study

provides preliminary proof for the anti-inflammatory of ASAC-CDs and its alleviation of ALI side effects caused by LPS. Be that as it may, further research is required to determine the underlying mechanism and bioactivity.

Conclusions

In summary, we succeeded in synthesizing and segregating novel CDs with low harmfulness through one-step pyrolysis of ASA. Within the LPS-induced ALI demonstrate in rats, ASAC-CDs prepared with small size and rich chemical groups have noteworthy anti-inflammatory impacts, which are to begin with illustrated to be related to diminish the levels of inflammation cytokines including IL-6, IL-1β and TNF-α and increase the contents of IL-10 in serum, and can moreover diminish the inflammation of the lungs to a certain degree. As a result of this work, ASAC-CDs are anticipated to get to be a reasonable elective for the treatment of ALI. This study provides a vital basis for the application of ASAC-CDs in clinical anti-pneumonia, and lays an experimental foundation for the advancement and application of ASAC-CDs.

Data Sharing Statement

The data that support the findings of this study are available from the corresponding authors upon reasonable request.

Acknowledgments

This work was supported by the Classical Prescription Basic Research Team of Beijing University of Chinese Medicine. The authors have no other relevant affiliations or financial involvement with any organisation or entity with a financial interest in or financial conflict with the subject matter or materials discussed in the manuscript apart from those disclosed.

Disclosure

The authors report no conflicts of interest for this work.

References

1. Xiao K, He W, Guan W, et al. Mesenchymal stem cells reverse EMT process through blocking the activation of NF-κB and Hedgehog pathways in LPS-induced acute lung injury. *Cell Death Dis*. 2020;11(10):863. doi:10.1038/s41419-020-03034-3
2. Ye R, Liu Z. ACE2 exhibits protective effects against LPS-induced acute lung injury in mice by inhibiting the LPS-TLR4 pathway. *Exp Mol Pathol*. 2020;113:104350. doi:10.1016/j.yexmp.2019.104350
3. Wu D, Zhang H, Wu Q, et al. Sestrin 2 protects against LPS-induced acute lung injury by inducing mitophagy in alveolar macrophages. *Life Sci*. 2021;267:118941. doi:10.1016/j.lfs.2020.118941
4. Feng B, Zhu J, Xu Y, et al. Immunosuppressive effects of mesenchymal stem cells on lung B cell gene expression in LPS-induced acute lung injury. *Stem Cell Res Ther*. 2020;11(1):418. doi:10.1186/s13287-020-01934-x
5. Zhang Z, Luo Z, Bi A, et al. Compound edaravone alleviates lipopolysaccharide (LPS)-induced acute lung injury in mice. *Eur J Pharmacol*. 2017;811:1–11. doi:10.1016/j.ejphar.2017.05.047
6. Mishra V, Patil A, Thakur S, et al. Carbon dots: emerging theranostic nanoarchitectures. *Drug Discov Today*. 2018;23(6):1219–1232. doi:10.1016/j.drudis.2018.01.006
7. Li L, Jiao X, Zhang Y, et al. Green synthesis of fluorescent carbon dots from Hongcaitai for selective detection of hypochlorite and mercuric ions and cell imaging. *Sensor Actuat B-Chem*. 2018;263:426–435. doi:10.1016/j.snb.2018.02.141
8. Li Y, Li S, Wang Y, et al. Electrochemical synthesis of phosphorus-doped graphene quantum dots for free radical scavenging. *Phys Chem Chem Phys*. 2017;19(18):11631–11638. doi:10.1039/c6cp06377b
9. Tong T, Hu H, Zhou J, et al. Glycyrrhizic-acid-based carbon dots with high antiviral activity by multisite inhibition mechanisms. *Small*. 2020;16(13):e1906206. doi:10.1002/smll.201906206
10. Zhang M, Cheng J, Hu J, et al. Green Phellodendri Chinensis Cortex-based carbon dots for ameliorating imiquimod-induced psoriasis-like inflammation in mice. *J Nanobiotechnology*. 2021;19(1):105. doi:10.1186/s12951-021-00847-y
11. Li Y, Bi J, Liu S, et al. Presence and formation of fluorescence carbon dots in a grilled hamburger. *Food Funct*. 2017;8(7):2558–2565. doi:10.1039/c7fo00675f
12. Veltri F, Alessandro F, Scarcello A, et al. Porous carbon materials obtained by the hydrothermal carbonization of orange juice. *Nanomaterials*. 2020;10(4):655. doi:10.3390/nano10040655
13. Yan X, Zhao Y, Luo J, et al. Hemostatic bioactivity of novel Pollen Typhae Carbonisata-derived carbon quantum dots. *J Nanobiotechnology*. 2017;15(1):60. doi:10.1186/s12951-017-0296-z
14. Wang S, Zhang Y, Kong H, et al. Antihyperuricemic and anti-gouty arthritis activities of Aurantii fructus immaturus carbonisata-derived carbon dots. *Nanomedicine*. 2019;14(22):2925–2939. doi:10.2217/nnm-2019-0255
15. Wei X, Li L, Liu J, et al. Green synthesis of fluorescent carbon dots from gynostemma for bioimaging and antioxidant in zebrafish. *ACS Appl Mater Interfaces*. 2019;11(10):9832–9840. doi:10.1021/acsami.9b00074
16. Dong Z, Xu R, Guan L, et al. Establishment of fingerprints of semen armeniacae amarum and its quality evaluation. *Chin J Exp Trad Med Formulae*. 2016;22(11):60–63. doi:10.13422/j.cnki.syfjx.2016110060
17. Ding C, Cao X, Zhang C, et al. Rare earth ions enhanced near infrared fluorescence of Ag_2S quantum dots for the detection of fluoride ions in living cells. *Nanoscale*. 2017;9(37):14031–14038. doi:10.1039/c7nr04436d
18. Yang L, Jiang W, Qiu L, et al. One pot synthesis of highly luminescent polyethylene glycol anchored carbon dots functionalized with a nuclear localization signal peptide for cell nucleus imaging. *Nanoscale*. 2015;7(14):6104–6113. doi:10.1039/c5nr01080b
19. Jia P, Yu L, Tao C, Dai G, Zhang Z, Liu S. Chitosan oligosaccharides protect nucleus pulposus cells from hydrogen peroxide-induced apoptosis in a rat experimental model. *Biomed Pharmacother*. 2017;93:807–815. doi:10.1016/j.biopha.2017.06.101
20. Hu J, Lai J, Zhou W, et al. Hypothermia alleviated LPS-induced acute lung injury in Rat models through TLR2/MyD88 pathway. *Exp Lung Res*. 2018;44(8–9):397–404. doi:10.1080/01902148.2018.1557299
21. Turhan AH, Atıcı A, Muşlu N, et al. The effects of pentoxifylline on lung inflammation in a rat model of meconium aspiration syndrome. *Exp Lung Res*. 2012;38(5):250–255. doi:10.3109/01902148.2012.676704
22. Liu X, Wang Y, Yan X, et al. Novel Phellodendri Cortex (Huang Bo)-derived carbon dots and their hemostatic effect. *Nanomedicine*. 2018;13(4):391–405. doi:10.2217/nnm-2017-0297

23. Ma W, Li W, Liu R, et al. Carbon dots and AIE molecules for highly efficient tandem luminescent solar concentrators. *Chem Commun (Camb)*. 2019;55(52):7486–7489. doi:10.1039/c9cc02676b
24. Wang L, Bi Y, Hou J, et al. Facile, green and clean one-step synthesis of carbon dots from wool: application as a sensor for glyphosate detection based on the inner filter effect. *Talanta*. 2016;160:268–275. doi:10.1016/j.talanta.2016.07.020
25. Wu J, Zhang M, Cheng J, et al. Effect of lonicerae japonicae flos carbonisata-derived carbon dots on rat models of fever and hypothermia induced by lipopolysaccharide. *Int J Nanomedicine*. 2020;15:4139–4149. doi:10.2147/IJN.S248467
26. Jahanbakhshi M, Habibi B. A novel and facile synthesis of carbon quantum dots via salep hydrothermal treatment as the silver nanoparticles support: application to electroanalytical determination of H_2O_2 in fetal bovine serum. *Biosens Bioelectron*. 2016;81:143–150. doi:10.1016/j.bios.2016.02.064
27. Zhang J, Niu A, Li J, et al. In vivo characterization of hair and skin derived carbon quantum dots with high quantum yield as long-term bioprobes in zebrafish. *Sci Rep*. 2016;6(1):37860. doi:10.1038/srep37860
28. Manchala S, Gandamalla A, Vempuluru NR, et al. High potential and robust ternary LaFeO3/CdS/carbon quantum dots nanocomposite for photocatalytic H2 evolution under sunlight illumination. *J Colloid Interface Sci*. 2021;583:255–266. doi:10.1016/j.jcis.2020.08.125
29. Wang Z, Liu J, Wang W, et al. Photoluminescent carbon quantum dot grafted silica nanoparticles directly synthesized from rice husk biomass. *J Mater Chem B*. 2017;5(24):4679–4689. doi:10.1039/c7tb00811b
30. Shen J, Shang S, Chen X, et al. Highly fluorescent N, S-co-doped carbon dots and their potential applications as antioxidants and sensitive probes for Cr (VI) detection. *Sensor Actuat B-Chem*. 2017;248:92–100. doi:10.1016/j.snb.2017.03.123
31. Cheng J, Zhang M, Sun Z, et al. Hemostatic and hepatoprotective bioactivity of Junci Medulla Carbonisata-derived Carbon Dots. *Nanomedicine*. 2019;14(4):431–446. doi:10.2217/nnm-2018-0285
32. Zhang Y, Wang S, Lu F, et al. The neuroprotective effect of pretreatment with carbon dots from Crinis Carbonisatus (carbonized human hair) against cerebral ischemia reperfusion injury. *J Nanobiotechnology*. 2021;19(1):257. doi:10.1186/s12951-021-00908-2
33. Zhang M, Cheng J, Sun Z, et al. Protective effects of carbon dots derived from phellodendri chinensis cortex carbonisata against deinagkistrodon acutus venom-induced acute kidney injury. *Nanoscale Res Lett*. 2019;14(1):377. doi:10.1186/s11671-019-3198-1
34. Docter D, Distler U, Storck W, et al. Quantitative profiling of the protein coronas that form around nanoparticles. *Nat Protoc*. 2014;9(9):2030–2044. doi:10.1038/nprot.2014.139
35. Blume JE, Manning WC, Troiano G, et al. Rapid, deep and precise profiling of the plasma proteome with multi-nanoparticle protein Corona. *Nat Commun*. 2020;11(1):3662. doi:10.1038/s41467-020-17033-7
36. Mao S, Chang J, Pu H, et al. Two-dimensional nanomaterial-based field-effect transistors for chemical and biological sensing. *Chem Soc Rev*. 2017;46(22):6872–6904. doi:10.1039/c6cs00827e
37. Mishra V, Patil A, Thakur S, et al. Carbon dots: emerging theranostic nanoarchitectures. *Drug Discov Today*. 2018;23(6):1219–1232. doi:10.1016/j.drudis.2018.01.006
38. Lin CJ, Chang L, Chu HW, et al. High amplification of the antiviral activity of curcumin through transformation into carbon quantum dots. *Small*. 2019;15(41):e1902641. doi:10.1002/smll.201902641
39. Wu F, Yue L, Yang L, et al. Ln(III) chelates-functionalized carbon quantum dots: synthesis, optical studies and multimodal bioimaging applications. *Colloids Surf B Biointerfaces*. 2019;175:272–280. doi:10.1016/j.colsurfb.2018.11.054
40. Duan Q, Jia Y, Qin Y, et al. Narciclasine attenuates LPS-induced acute lung injury in neonatal rats through suppressing inflammation and oxidative stress. *Bioengineered*. 2020;11(1):801–810. doi:10.1080/21655979.2020.1795424
41. Hu X, Li H, Fu L, et al. The protective effect of hyperin on LPS-induced acute lung injury in mice. *Microb Pathog*. 2019;127:116–120. doi:10.1016/j.micpath.2018.11.048
42. Wang X, Wong K, Ouyang W, et al. Targeting IL-10 family cytokines for the treatment of human diseases. *Cold Spring Harb Perspect Biol*. 2019;11(2):a028548. doi:10.1101/cshperspect.a028548
43. Ju M, Liu B, He H, et al. MicroRNA-27a alleviates LPS-induced acute lung injury in mice via inhibiting inflammation and apoptosis through modulating TLR4/MyD88/NF-κB pathway. *Cell Cycle*. 2018;17(16):2001–2018. doi:10.1080/15384101.2018.1509635
44. Zhu DZ, Wang YT, Zhuo YL, et al. Fucoidan inhibits LPS-induced acute lung injury in mice through regulating GSK-3β-Nrf2 signaling pathway. *Arch Pharm Res*. 2020;43(6):646–654. doi:10.1007/s12272-020-01234-1
45. Ali H, Khan A, Ali J, et al. Attenuation of LPS-induced acute lung injury by continentalic acid in rodents through inhibition of inflammatory mediators correlates with increased Nrf2 protein expression. *BMC Pharmacol Toxicol*. 2020;21(1):81. doi:10.1186/s40360-020-00458-7
46. Huang CY, Deng JS, Huang WC, et al. Attenuation of Lipopolysaccharide-Induced Acute Lung Injury by Hispolon in Mice, Through Regulating the TLR4/PI3K/Akt/mTOR and Keap1/Nrf2/HO-1 Pathways, and Suppressing Oxidative Stress-Mediated ER Stress-Induced Apoptosis and Autophagy. *Nutrients*. 2020;12(6):1742. doi:10.3390/nu12061742
47. Zhang Y, Yu W, Han D, et al. L-lysine ameliorates sepsis-induced acute lung injury in a lipopolysaccharide-induced mouse model. *Biomed Pharmacother*. 2019;118:109307. doi:10.1016/j.biopha.2019.109307
48. Meng L, Li L, Lu S, et al. The protective effect of dexmedetomidine on LPS-induced acute lung injury through the HMGB1-mediated TLR4/NF-κB and PI3K/Akt/mTOR pathways. *Mol Immunol*. 2018;94:7–17. doi:10.1016/j.molimm.2017.12.008